Physical Climate Response to a Reduction of Anthropogenic Climate Forcing

Arindam Samanta* and Bruce T. Anderson

Boston University, Boston, Massachusetts

Sangram Ganguly

BAERI/NASA Ames Research Center, Moffett Field, California

Yuri Knyazikhin

Boston University, Boston, Massachusetts

Ramakrishna R. Nemani

NASA Ames Research Center, Moffett Field, California

Ranga B. Myneni

Boston University, Boston, Massachusetts

Received 5 January 2010; accepted 26 April 2010

ABSTRACT: Recent research indicates that the warming of the climate system resulting from increased greenhouse gas (GHG) emissions over the next century will persist for many centuries after the cessation of these emissions, principally because of the persistence of elevated atmospheric carbon dioxide (CO_2) concentrations and their attendant radiative forcing. However, it is unknown

* Corresponding author address: Arindam Samanta, Department of Geography and Environment, Boston University, 675 Commonwealth Avenue, Boston, MA 02215.

E-mail address: arindam.sam@gmail.com

DOI: 10.1175/2010EI325.1

whether the responses of other components of the climate system—including those related to Greenland and Antarctic ice cover, the Atlantic thermohaline circulation, the West African monsoon, and ecosystem and human welfare—would be reversed even if atmospheric CO_2 concentrations were to recover to 1990 levels. Here, using a simple set of experiments employing a current-generation numerical climate model, the authors examine the response of the physical climate system to decreasing CO_2 concentrations following an initial increase. Results indicate that many characteristics of the climate system, including global temperatures, precipitation, soil moisture, and sea ice, recover as CO_2 concentrations decrease. However, other components of the Earth system may still exhibit nonlinear hysteresis. In these experiments, for instance, increases in stratospheric water vapor, which initially result from increased CO_2 concentrations, remain present even as CO_2 concentrations recover. These results suggest that identification of additional threshold behaviors in response to human-induced global climate change should focus on subcomponents of the full Earth system, including cryosphere, biosphere, and chemistry.

KEYWORDS: Forcing; Feedback; Climate

1. Introduction

Increasingly, it is recognized that current and future greenhouse gas (GHG) emissions have a significant likelihood of producing increased global temperatures—and concurrent climate change—above 2°C (Parry et al. 2009), which is likely to result in significant and dangerous physical, biological, and socioeconomic impacts (Parry et al. 2007). As such international efforts are presently underway to reduce these future GHG emissions as a means of limiting human-induced global-scale temperature increases to 2°C, relative to the preindustrial era (Council of the European Union 2005). However, the efficacy of these proposed efforts is unknown as there is scant evidence, save for a few studies (e.g., Nakashiki et al. 2006; Tsutsui et al. 2007; Matthews and Caldeira 2008; Lowe et al. 2009; Solomon et al. 2009), that any subsequent reduction of atmospheric GHG concentrations would reverse or mitigate the intervening climate changes (Solomon et al. 2007) or their impacts (Parry et al. 2007).

To explicitly examine the response of the climate system to decreasing GHG concentrations, we performed a simple set of experiments with a coupled atmosphere–ocean general circulation model (GCM), in which the carbon dioxide (CO_2) concentrations were increased from 350 to 700 ppmv (parts per million by volume) and then decreased back to 350 ppmv (Figure 1a). The 350-ppmv CO_2 concentration is the desired stabilization level (Hansen et al. 2008) and roughly corresponds to the base year 1990 CO_2 concentration (355 ppmv) adopted by the Kyoto Protocol and the Intergovernmental Panel on Climate Change (IPCC) Special Report on Emissions Scenarios (SRES) (Solomon et al. 2007). The intervening 350-ppmv CO_2 increase corresponds to a radiative forcing of 3.6 W m^{-2}, which is well within the realm of what can be expected in the twenty-first century from anthropogenic contributions of radiatively active chemical constituents to the atmosphere, absent major emission cuts (Solomon et al. 2007). We recognize that this rate of decline in CO_2 is unrealistic, barring significant advancements in carbon sequestration technologies (Metz et al. 2005); however, this experiment helps us determine the nonlinear response of the climate system, separate from the nonlinear radiative forcing associated with the long-lived decay of atmospheric

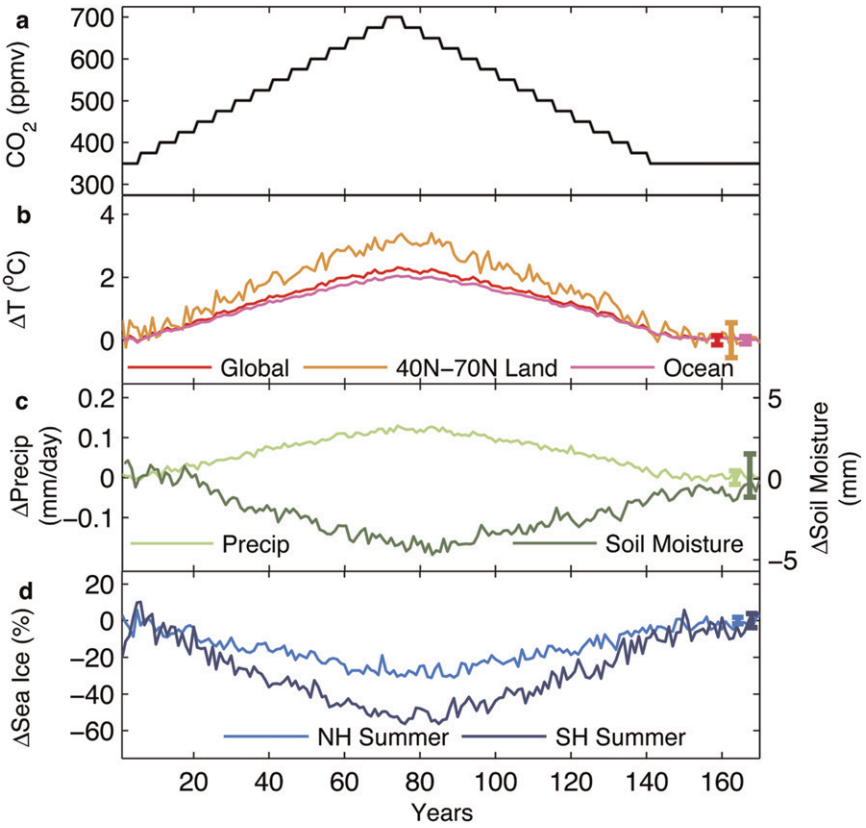

Figure 1. (a) Atmospheric CO_2 concentration used in the experimental runs. Changes in ensemble-mean climate variables relative to 100-yr mean values derived from the same model but forced with atmospheric CO_2 concentrations fixed at 350 ppmv (control run). (b) Annual mean surface temperature (°C) averaged over the globe (red), oceans (magenta), and Northern Hemisphere extratropical land surfaces (orange). (c) Annual mean globally averaged precipitation (mm day^{-1}; light green) and soil moisture (mm; dark green). (d) Fractional coverage of summertime mean sea ice extent over the Arctic Ocean from 60° to 90°N during July–September (%; light blue) and the Southern Ocean (Antarctic Ocean) from 60° to 90°S during January–March (%; deep blue). Also shown are ±two standard deviation (vertical bars) of the 100-yr control run outputs for each variable, estimated using a 1000 (100 year) member bootstrapping scheme.

CO_2 concentration, as investigated by others (Matthews and Caldeira 2008; Lowe et al. 2009; Solomon et al. 2009).

2. Model and experiments

We use version 3 of the National Center for Atmospheric Research Community Atmosphere Model (NCAR CAM 3.0). This GCM consists of a fully dynamic atmosphere model (CAM 3.0) coupled to an interactive land model [Community

Land Model (CLM) 3.0], a thermodynamic sea ice model, and a slab ocean model (Collins et al. 2006). The atmosphere (CAM 3.0) and land (CLM 3.0) models are part of the Community Climate System Model, version 3 (CCSM3; Kiehl et al. 2006). This GCM configuration allows short equilibration times while still attaining representative climate states in response to a given forcing (Kiehl et al. 2006). As such, slab ocean versions of coupled atmosphere–ocean GCMs similar to this one are used in a variety of climate sensitivity studies (e.g., Kiehl et al. 2006; Gregory and Webb 2008; Bala et al. 2008).

We perform (i) a 150-yr control run with CO_2 concentrations fixed at 350 ppmv and (ii) three transient ensemble runs, each initialized off the control run, in which the CO_2 concentrations are increased from 350 to 700 ppmv (ascending phase) and then decreased back to 350 ppmv (descending phase) in steps of 25 ppmv every 5 years (Figure 1a). At that point, the CO_2 concentration is held fixed at 350 ppmv for the next 30 years (Figure 1a). The three ensemble members are initialized at 1-yr intervals so as to incorporate interannual variability. These simulations start from the 13th, 14th, and 15th year of the control run, respectively. All model simulations are performed at T42 ($\sim 2.8^\circ \times 2.8^\circ$ horizontal resolution) spectral truncation with 26 layers in the vertical extending from the surface to approximately 3 hPa. Changes in the climate response to imposed CO_2 concentrations are calculated as the difference between the ensemble-mean value taken from the transient simulations and a 100-yr (years 21–120) mean value derived from the control run.

3. Results

Projections from the model system indicate that the global annual mean surface temperature is 2.3°C warmer (3.4°C in the high-latitude land areas) at 700-ppmv CO_2 compared to the control (Figure 1b). Global mean precipitation increases by approximately 0.14 mm day^{-1} (Figure 1c). The loss in summer sea ice extent is about 30% in the Arctic and 55% in the Antarctic (Figure 1d). The changes in temperature and precipitation are in agreement with those reported in current literature (see A1B scenario from Solomon et al. 2007; Kiehl et al. 2006), although this model system may underestimate changes in sea ice extent due to the lack of ocean and sea ice dynamics. Further we find that both temperature and precipitation return to their initial levels as CO_2 concentration is decreased from 700 to 350 ppmv and held constant for 30 years. The amplification of warming in the high latitudes also disappears. Soil moisture and summer sea ice extent in the Northern and Southern Hemispheres recover within this 30-yr period as well (Figures 1c and 1d).

Overall, the physical climate system simulated by the numerical model suggests that global climate parameters—temperature, precipitation, soil moisture, and sea ice—return to their initial values soon after the CO_2 concentrations do. To better understand the quasi-linear response of the physical climate system to increasing and decreasing CO_2 concentrations, we examine metrics related to the prominent feedback mechanisms active on the time scales over which the CO_2 concentrations are occurring, including surface (snow and sea ice) albedo, clouds, water vapor/lapse rate, and radiative cooling (e.g., Bony et al. 2006). To show the response of surface albedo, we calculated changes in Northern Hemisphere extratropical springtime surface albedo, modulated by the dependence of planetary albedo on surface albedo and multiplied by solar insolation (as in Qu and Hall 2006), and plotted it as a

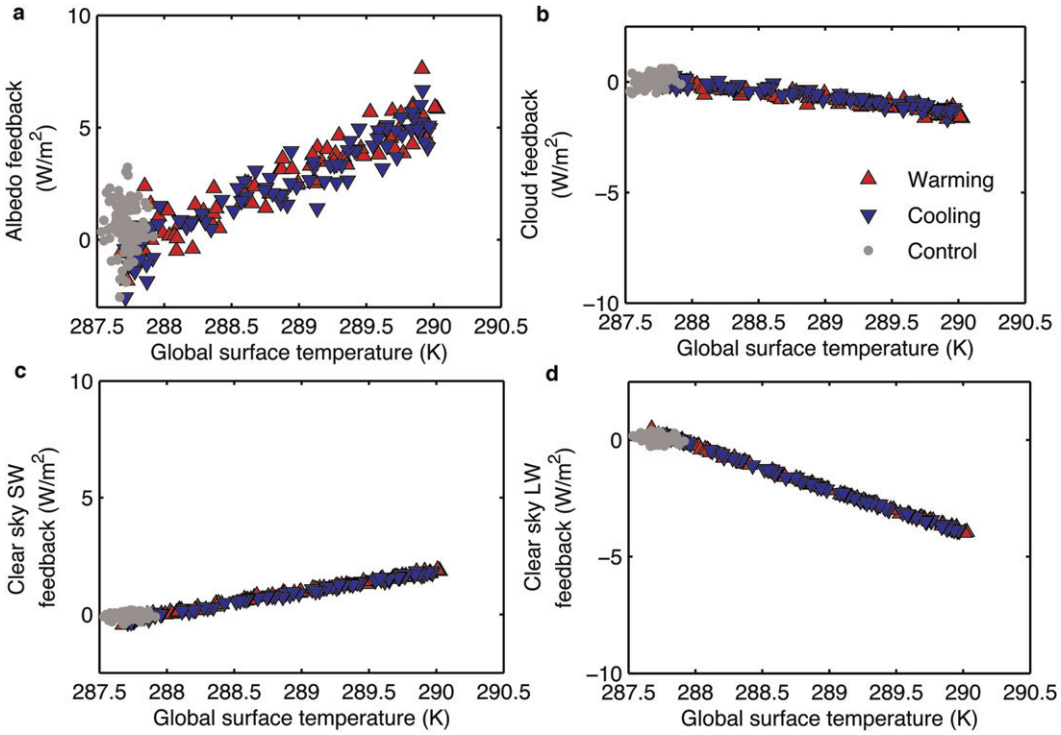

Figure 2. (a) Change in Northern Hemisphere extratropical spring season (March–May) absorbed shortwave radiation (W m^{-2}) at the surface plotted as a function of global annual mean surface temperature (K) during (100 years) control run (gray), and ascending phase (red) and descending phase (blue) of CO_2 concentrations seen in Figure 1a. Absorbed shortwave radiation is calculated using the mean surface albedo multiplied by the fractional dependence of planetary albedo on surface albedo (W m^{-2}) (Qu and Hall 2006). (b)–(d) Same as in (a), but for global annual mean cloud radiative forcing (W m^{-2}), global annual mean clear-sky SW feedback (W m^{-2}), and global annual mean clear-sky LW feedback (W m^{-2}). All lines are shifted such that initial values start at 0.

function of global mean surface temperature (Figure 2a). Overall, there is a linear decrease (increase) of reflected incoming solar radiation with an increase (decrease) in surface temperature (the associated feedback is plotted here as a positive increase in absorbed radiation). This linear behavior of Northern Hemisphere snow cover is attributable to strong thermodynamic coupling with surface temperatures (Hall 2004) during both warming (ascending) and cooling (descending) phases of the climate system.

Cloud feedbacks are estimated by quantifying changes in cloud radiative forcing (Cess et al. 1996), which is a measure of the impact of clouds upon the top-of-atmosphere (TOA) radiation balance. The net effect of clouds is to cool the simulated climate system (Kiehl et al. 2006), with increased cooling under warmer climates and reduced cooling under colder climates (Figure 2b). Overall, though, the cloud radiative forcing adjusts quasi-linearly with surface temperature as well.

Clear-sky feedbacks can be estimated using the approach in Forster and Taylor (Forster and Taylor 2006) and Gregory and Webb (Gregory and Webb 2008) based upon separate estimates of the transient clear-sky shortwave [SW; Equation (1a)] and longwave [LW; Equation (1b)] top-of-atmosphere radiation budget:

$$F_{\mathrm{SW}}^{\mathrm{CLR}} = Q_{\mathrm{SW}}^{\mathrm{CLR}} - N_{\mathrm{SW}}^{\mathrm{CLR}}, \tag{1a}$$

$$F_{\mathrm{LW}}^{\mathrm{CLR}} = Q_{\mathrm{LW}}^{\mathrm{CLR}} - N_{\mathrm{LW}}^{\mathrm{CLR}}, \tag{1b}$$

where $F_{\mathrm{SW}}^{\mathrm{CLR}}$ ($F_{\mathrm{LW}}^{\mathrm{CLR}}$) is the annual global mean clear-sky SW (LW) climate response (equivalent to the feedback strength); $N_{\mathrm{SW}}^{\mathrm{CLR}}$ ($N_{\mathrm{LW}}^{\mathrm{CLR}}$) is the change in annual global mean TOA net clear-sky SW (LW) flux relative to the 100-yr mean value derived from the control run (cf. section 2); and $Q_{\mathrm{SW}}^{\mathrm{CLR}}$ ($Q_{\mathrm{LW}}^{\mathrm{CLR}}$) is the annual global mean SW (LW) transient forcing. As in Forster and Taylor (Forster and Taylor 2006), we can estimate the annual global mean SW (LW) transient forcing as

$$Q_{\mathrm{SW}}^{\mathrm{CLR}} = f(-0.22)\ln(C/C_o), \tag{2a}$$

$$Q_{\mathrm{LW}}^{\mathrm{CLR}} = f(5.57)\ln(C/C_o), \tag{2b}$$

where f is the ratio of our model's $2 \times CO_2$ (300–750 ppm) net (stratosphere) adjusted clear-sky forcing (3.75 W m^{-2}) to the radiative forcing estimate (3.7 W m^{-2}) in Myhre et al. (Myhre et al. 1998). In the transient model simulation C is the time-varying atmospheric CO_2 concentration and C_o is the control CO_2 concentration (350 ppm).

Solving for $F_{\mathrm{SW}}^{\mathrm{CLR}}$ ($F_{\mathrm{LW}}^{\mathrm{CLR}}$), we can calculate the strength of both the clear-sky SW and LW feedbacks (Figures 2c and 2d). In agreement with the albedo feedback results, the clear-sky SW feedback is positive. In contrast, the clear-sky LW feedback, which incorporates the negative feedback associated with enhanced blackbody emissions from a warmer atmosphere along with the positive feedback associated with water vapor/lapse rate changes, is negative, in agreement with similar studies (e.g., Gregory and Webb 2008). Importantly, like the surface albedo and cloud radiative feedbacks, both the clear-sky SW and LW feedbacks change linearly with surface temperature.

4. Discussion

Above, we find that prominent global-scale radiative feedback mechanisms associated with snow–ice albedo, clouds, and clear-sky conditions all show a quasi-linear response to changes in radiative forcing. However, further investigation suggests that changes in individual radiative flux terms do not necessarily show such quasi-linear behavior. In particular, the outgoing TOA clear-sky longwave flux increases linearly with increasing temperatures but remains elevated even as global temperatures decrease, producing an asymmetric time trajectory (Figure 3a).

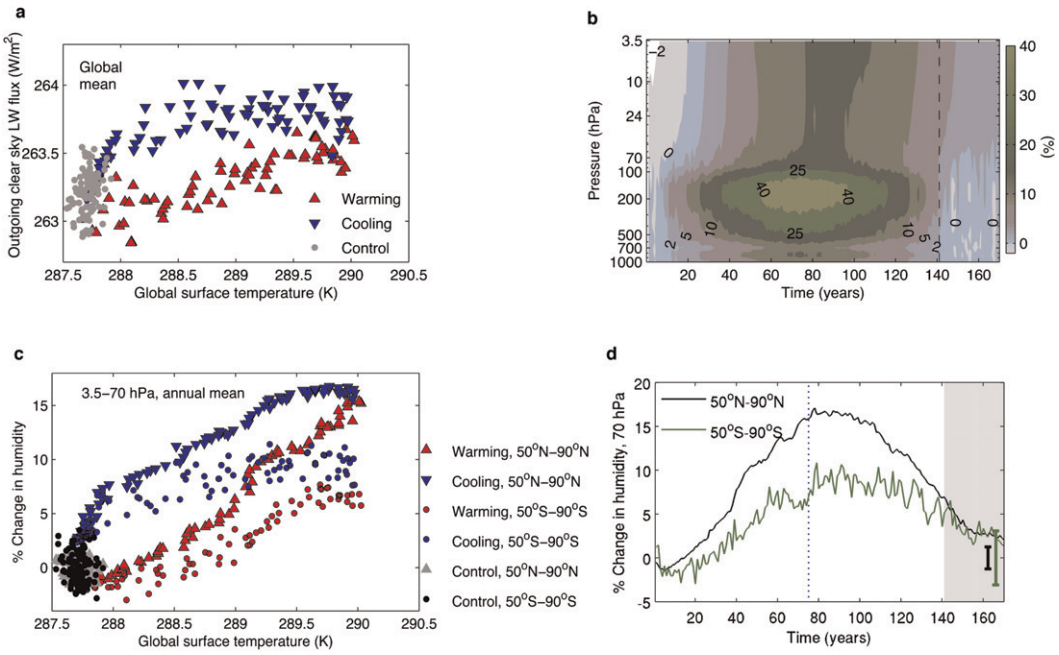

Figure 3. (a) Global annual mean outgoing TOA clear-sky LW flux (W m^{-2}) plotted as a function of global annual mean surface temperature (K) during (100 years) control run (gray), and ascending phase (red) and descending phase (blue) of CO_2 concentrations seen in Figure 1a. (b) Height (pressure)–time contour of percentage change (%) in global annual mean specific humidity. Dashed line marks the year when CO_2 is stabilized at 350 ppmv. (c) Percentage change (%) in annual mean stratospheric (3.5–70 hPa) specific humidity averaged over 50°–90°N (triangles) and 50°–90°S (circles), plotted as a function of global annual mean surface temperature (K) during (100 years) control run (gray and black), and ascending phase (red) and descending phase (blue) of CO_2 concentrations seen in Figure 1a. (d) Percentage change (%) in annual mean lower stratospheric (70 hPa) specific humidity averaged over 50°–90°N (black) and 50°–90°S (dark green). Dotted (blue) line marks the year when reduction of CO_2 from 700 ppmv begins. Shading shows the time period during which CO_2 is stabilized at 350 ppmv. Also shown are ±two standard deviation (vertical bars) of the 100-yr control run outputs of annual mean lower stratospheric (70 hPa) specific humidity averaged over 50°–90°N (black) and 50°–90°S (dark green), estimated using a 1000 (100 years) member bootstrapping scheme.

While this asymmetric response does not necessarily impact the global mean surface temperatures (see Figure 1; also Bony et al. 2006; Stuber et al. 2001), it does suggest that certain components of the full Earth system could experience nonlinear hysteresis as CO_2 concentrations return to their current levels. We investigate the TOA clear-sky LW component in more detail here.

Changes in the outgoing clear-sky LW flux arise from changes in both water vapor and lapse rate. Linear changes in temperature throughout the troposphere and

lower stratosphere (not shown) rule out an asymmetric contribution of lapse rate profiles. In addition, changes in the tropospheric water vapor are symmetric (Figure 3b). However, water vapor in the stratosphere, particularly in the high latitudes, evolves nonlinearly (Figure 3b), leading to the asymmetric evolution of the TOA outgoing clear-sky LW flux. At the peak of warming, the stratospheric water vapor increase is approximately 15%–20% (10%–12%) in the northern (southern) high latitudes (Figure 3c). The water vapor budget of the stratosphere is controlled by entry through the tropical lower stratosphere (Brewer 1949) and downwelling in high latitudes (Holton et al. 1995) (our experimental setup precludes any contributions from methane oxidation; Le Texier et al. 1988). During the ascending phase of CO_2 concentrations, a combination of increasing tropical cold point temperature (CPT, not shown) (e.g., Oman et al. 2008) and accelerating Brewer–Dobson circulation (e.g., Butchart et al. 2006; McLandress and Shepherd 2009), result in enhanced injection of water vapor near the tropical tropopause and subsequent buildup within the stratosphere.

During the descending phase of CO_2 concentrations, there is a linear decrease in CPT (not shown); however, the high-latitude water vapor trajectory has a significant positive offset, particularly over the Southern Hemisphere where it does not begin to decrease until temperatures approach their initial levels (Figures 3c and 3d). Why should this be so? We hypothesize that during the cooling phase, the removal of the excess water vapor is controlled by the imbalance between the upwelling and downwelling of the Brewer–Dobson circulation (Holton et al. 1995) (it is important to note that the rate of removal is *not* related to the residence time of stratospheric air—approximately 2 years—which only determines the average time a given parcel remains within the stratosphere, not necessarily the time rate of change of mass within the stratosphere). Analogous to the removal of excess CO_2 from the troposphere (Solomon et al. 2009), the result is a long-lived decay of water vapor even after 30 years of equilibrium forcing (Figure 3d), albeit with significant interannual to decadal fluctuations (Solomon et al. 2010). As for the asymmetries between the two hemispheres—including differences in the overall amplitude, year-to-year variability, and rate of decrease (Figures 3c and 3d)—these most likely arise from greater wave breaking in the Northern Hemisphere high latitudes leading to enhanced mixing of tropospheric air from below (e.g., McIntyre and Palmer 1983; Baldwin et al. 2003).

To validate these results, however, a whole-atmosphere model incorporating full stratospheric physics and chemistry (Garcia and Randel 2008) will need to be employed. In addition, such an advanced atmospheric model would help quantify the influence of excess stratospheric water vapor upon both the thermodynamics and dynamics of the extratropical stratosphere and troposphere, as well as the evolution and recovery of stratospheric ozone (Shindell 2001; Solomon et al. 2010).

Further, the use of a slab ocean GCM, typically used for climate sensitivity studies (e.g., Kiehl et al. 2006; Gregory and Webb 2008; Bala et al. 2008), precludes the effects of large thermal inertia of the global ocean upon the simulated physical climate system. These effects consist primarily of lags in the response of the simulated climate system to changes in radiative forcings imposed by atmosphere–ocean GCMs (AOGCMs) during transient climate change simulations (e.g., Wetherald et al. 2001; Wigley 2005; Meehl et al. 2005). Such lags are functions

of the climate sensitivity and ocean heat uptake of AOGCM's as well as the imposed forcing scenarios (e.g., Wetherald et al. 2001; Meehl et al. 2005) and are known to "commit" the climate system to further warming even after GHG concentrations (radiative forcings) are stabilized (e.g., Wetherald et al. 2001; Wigley 2005; Meehl et al. 2005). One reason we chose to plot the radiative flux terms (Figures 2 and 3) as a function of temperature as opposed to CO_2 concentrations is to account for this lag in the transient climate change response of slab ocean GCMs and AOGCMs. In addition, even in the presence of lags, surface temperature and precipitation simulated by AOGCMs are reported to change linearly with radiative forcings (Tsutsui et al. 2007). Therefore, the linear trajectory of surface temperature, precipitation, and soil moisture vis-à-vis increased and decreased radiative forcing, as shown here, may be representative, at least qualitatively, of those found in AOGCMs after accounting for the lagged response within AOGCMs [which typically is on the order of decades (Wetherald et al. 2001; Tsutsui et al. 2007)]. On the other hand, changes in sea ice extent found here are less reliable because of the absence of ocean and sea ice dynamics. In addition to the follow-up whole-atmosphere model studies of nonlinear stratospheric water vapor responses, it will also be interesting to perform further experiments with AOGCMs to explicitly investigate the nature of ocean-induced lags and their effects on the response of the physical climate system to decreasing anthropogenic radiative forcings.

5. Conclusions

Overall, the physical climate system simulated by the numerical model shows a slightly lagged response to changing CO_2 concentrations. Importantly, most climate parameters return to their initial values soon after the CO_2 concentrations do. This quasi-linear evolution arises from the linear (albeit unrealistic; Solomon et al. 2009) nature of the imposed forcing, as well as the quasi-linear response of prominent feedback mechanisms associated with snow–ice albedo, clouds, water vapor/lapse rate, and radiative cooling. Similar results are not found in all components of the Earth system, however. In our study, stratospheric water vapor remains elevated despite decreasing tropospheric and stratospheric temperatures. It is still unknown whether potential changes to other physical subsystems—including Greenland and Antarctic ice cover, the Atlantic thermohaline circulation, and the West African monsoon (Solomon et al. 2007; Parry et al. 2007; Lenton et al. 2008)—and biological systems—including impacts to ecosystems and human welfare—accrued during the warming phase (Parry et al. 2007) will show similar nonlinear recoveries. Results presented here need to be tested for reliability using other modeling systems. They should also be investigated using climate models that incorporate additional components of the full Earth system.

Acknowledgments. We acknowledge support from A. Michaelis (NASA AMES Research Center), M. Dugan (Boston University), and R. Neale (National Center for Atmospheric Research).

References

Bala, G., P. B. Duffy, and K. E. Taylor, 2008: Impact of geoengineering schemes on the global hydrological cycle. *Proc. Natl. Acad. Sci. USA,* **105,** 7664–7669.

Baldwin, M. P., D. W. J. Thompson, E. F. Shuckburgh, W. A. Norton, and N. P. Gillett, 2003: Weather from the stratosphere? *Science,* **301,** 317–319.

Bony, S., and Coauthors, 2006: How well do we understand and evaluate climate change feedback processes? *J. Climate,* **19,** 3445–3482.

Brewer, A. W., 1949: Evidence for a world circulation provided by the measurements of helium and water vapor distribution in the stratosphere. *Quart. J. Roy. Meteor. Soc.,* **75,** 351–363.

Butchart, N., and Coauthors, 2006: Simulations of anthropogenic change in the strength of the Brewer-Dobson circulation. *Climate Dyn.,* **27,** 727–741.

Cess, R. D., and Coauthors, 1996: Cloud feedback in atmospheric general circulation models: An update. *J. Geophys. Res.,* **101,** 12 791–12 794.

Collins, W. D., and Coauthors, 2006: The formulation and atmospheric simulation of the Community Atmosphere Model Version 3 (CAM3). *J. Climate,* **19,** 2144–2161.

Council of the European Union, cited 2005: Presidency conclusions. Brussels European Council, 39 pp. [Available online at http://www.consilium.europa.eu/uedocs/cms_Data/docs/pressdata/en/ec/84335.pdf.]

Forster, P. M. D., and K. E. Taylor, 2006: Climate forcings and climate sensitivities diagnosed from coupled climate model integrations. *J. Climate,* **19,** 6181–6194.

Garcia, R. R., and W. J. Randel, 2008: Acceleration of the Brewer–Dobson circulation due to increases in greenhouse gases. *J. Atmos. Sci.,* **65,** 2731–2739.

Gregory, J., and M. Webb, 2008: Tropospheric adjustment induces a cloud component in CO_2 forcing. *J. Climate,* **21,** 58–71.

Hall, A., 2004: The role of surface albedo feedback in climate. *J. Climate,* **17,** 1550–1568.

Hansen, J., and Coauthors, 2008: Target atmospheric CO_2: Where should humanity aim? *Open Atmos. Sci. J.,* **2,** 217–231.

Holton, J. R., P. H. Haynes, M. E. McIntyre, A. R. Douglass, R. B. Rood, and L. Pfister, 1995: Stratosphere–troposphere exchange. *Rev. Geophys.,* **33,** 403–439.

Kiehl, J. T., C. A. Shields, J. J. Hack, and W. D. Collins, 2006: The climate sensitivity of the Community Climate System Model version 3 (CCSM3). *J. Climate,* **19,** 2584–2596.

Lenton, T. M., H. Held, E. Kriegler, J. W. Hall, W. Lucht, S. Rahmstorf, and H. J. Schellnhuber, 2008: Tipping elements in the Earth's climate system. *Proc. Natl. Acad. Sci. USA,* **105,** 1786–1793.

Le Texier, H., S. Solomon, and R. R. Garcia, 1988: The role of molecular hydrogen and methane oxidation in the water vapor budget of the stratosphere. *Quart. J. Roy. Meteor. Soc.,* **114,** 281–295.

Lowe, J. A., C. Huntingford, S. C. B. Raper, C. D. Jones, S. K. Liddicoat, and L. K. Gohar, 2009: How difficult is it to recover from dangerous levels of global warming? *Environ. Res. Lett.,* **4,** 014012.

Matthews, H. D., and K. Caldeira, 2008: Stabilizing climate requires near-zero emissions. *Geophys. Res. Lett.,* **35,** L04705.

McIntyre, M. E., and T. N. Palmer, 1983: Breaking planetary-waves in the stratosphere. *Nature,* **305,** 593–600.

McLandress, C., and T. G. Shepherd, 2009: Simulated anthropogenic changes in the Brewer–Dobson circulation, including its extension to high latitudes. *J. Climate,* **22,** 1516–1540.

Meehl, G. A., W. M. Washington, W. D. Collins, J. M. Arblaster, A. X. Hu, L. E. Buja, W. G. Strand, and H. Y. Teng, 2005: How much more global warming and sea level rise? *Science,* **307,** 1769–1772.

Metz, B., O. Davidson, H. de Coninck, M. Loos, and L. Meyer, Eds., 2005: *IPCC Special Report on Carbon Dioxide Capture and Storage*. Cambridge University Press, 442 pp.

Myhre, G., E. J. Highwood, K. P. Shine, and F. Stordal, 1998: New estimates of radiative forcing due to well mixed greenhouse gases. *Geophys. Res. Lett.,* **25,** 2715–2718.

Nakashiki, N., D.-H. Kim, F. O. Bryan, Y. Yoshida, D. Tsumune, K. Maruyama, and H. Kitabata, 2006: Recovery of the thermohaline circulation under CO_2 stabilization and overshoot scenarios. *Ocean Modell.,* **15,** 200–217.

Oman, L., D. W. Waugh, S. Pawson, R. S. Stolarski, and J. E. Nielsen, 2008: Understanding the changes of stratospheric water vapor in coupled Chemistry–Climate Model simulations. *J. Atmos. Sci.,* **65,** 3278–3291.

Parry, M. L., O. F. Canziani, J. P. Palutikof, P. J. van der Linden, and C. E. Hanson, Eds., 2007: *Climate Change 2007: Impacts, Adaptation and Vulnerability.* Cambridge University Press, 976 pp.

——, J. Lowe, and C. Hanson, 2009: Overshoot, adapt and recover. *Nature,* **458,** 1102–1103.

Qu, X., and A. Hall, 2006: Assessing snow albedo feedback in simulated climate change. *J. Climate,* **19,** 2617–2630.

Shindell, D. T., 2001: Climate and ozone response to increased stratospheric water vapor. *Geophys. Res. Lett.,* **28,** 1551–1554.

Solomon, S., D. Qin, M. Manning, M. Marquis, K. Averyt, M. M. B. Tignor, H. L. Miller, Jr., and Z. Chen, Eds., 2007: *Climate Change 2007: The Physical Science Basis*. Cambridge University Press, 996 pp.

——, G. K. Plattner, R. Knutti, and P. Friedlingstein, 2009: Irreversible climate change due to carbon dioxide emissions. *Proc. Natl. Acad. Sci. USA,* **106,** 1704–1709.

——, K. Rosenlof, R. Portmann, J. Daniel, S. Davis, T. Sanford, and G. K. Plattner, 2010: Contributions of stratospheric water vapor to decadal changes in the rate of global warming. *Science,* **327,** 1219–1223.

Stuber, N., M. Ponater, and R. Sausen, 2001: Is the climate sensitivity to ozone perturbations enhanced by stratospheric water vapor feedback? *Geophys. Res. Lett.,* **28**(15), 2887–2890.

Tsutsui, J., Y. Yoshida, D. Kim, H. Kitabata, K. Nishizawa, N. Nakashiki, and K. Maruyama, 2007: Long-term climate response to stabilized and overshoot anthropogenic forcings beyond the twenty-first century. *Climate Dyn.,* **28,** 199–214.

Wetherald, R. T., R. J. Stouffer, and K. W. Dixon, 2001: Committed warming and its implications for climate change. *Geophys. Res. Lett.,* **28,** 1535–1538.

Wigley, T. M. L., 2005: The climate change commitment. *Science,* **307,** 1766–1769.